

# Efficient in-situ generation of photon-memory entanglement in a nonlinear cavity

Hoi-Kwan Lau,<sup>1,2</sup> Hong Qiao,<sup>1</sup> Aashish A. Clerk,<sup>1</sup> and Tian Zhong<sup>1</sup>

<sup>1</sup>*Pritzker School of Molecular Engineering, University of Chicago, Chicago, Illinois 60637, USA*

<sup>2</sup>*Department of Physics, Simon Fraser University, Burnaby, BC V5A 1S6, Canada*

(Dated: August 2, 2022)

Combining parametric driving and photon-atomic memory coupling within one optical cavity, we describe a scheme for in-situ generation of multimode photon-memory entanglement. We find that precise cavity impedance matching is neither required nor optimal to achieve high-rate entanglement for quantum networks. This protocol can be realized with existing technologies based on on-chip photonic cavities integrated with a rare-earth-ion doped quantum memory. The proposed scheme shows significant advantages in entanglement generation rates compared with start-of-the-art quantum memory protocols and experiments, with predicted Ebit generation rates of tens of MHz without ideal operating conditions. Such a photon-memory entanglement system offers a versatile resource for quantum interconnect applications.

*Introduction.*- Entanglement between itinerant optical photons and matter degrees of freedom is a fundamental resource for remote quantum interconnects, with imminent applications in quantum networks [1–3], quantum transduction [4, 5], quantum-enhanced telescopes [6], and distributed quantum computation [7–9]. Using Raman transitions, the well-known Duan-Lukin-Cirac-Zoller (DLCZ) protocol generates one entangled bit (Ebit) between two remote atomic ensembles, with built-in entanglement purification and noise resilience [10]. This protocol was extended to multimode operation by combining an EPR photon pair source with a broadband quantum memory realized via inhomogeneously broadened atomic ensembles in solids, leading to orders of magnitude speedup of the Ebit generation rate and reduced experimental complexities [11]. While these protocols are long established, experimental demonstrations of multi-mode entanglement between two remote atomic memories were only achieved very recently [12, 13]. Long-standing challenges hampering this scheme include photon loss and bandwidth mismatch at the interface between itinerant optical modes and the stationary memory degree of freedom. For instance, in the experiments employing separate photon sources and memories, the entanglement generation rates are limited even over a short fiber distance [12, 13]. One strategy to circumvent this loss at the light-matter interface is to use an atom-containing optical cavity with engineered impedance matching conditions [14, 15]. However, such a cavity-enhanced photon-memory interface introduces further complexities, and its robust implementation remains an open challenge.

In this Letter we propose a scheme for efficient multimode entanglement generation between optical photons and an atomic memory within a nonlinear cavity. By parametrically driving the cavity, we produce non-degenerate photon pairs (i.e. signal and idler photons), with one of the photons (i.e. signal) having spectral overlap with an inhomogeneously broadened atomic ensemble. By constructing an equivalent circuit representation

of the steady-state input-output relations, we uncover the basic structure of the resulting multi-partite entanglement generated between the atomic and two photonic degrees of freedom. We find that our scheme is capable of generating photon-memory entanglement over a broad spectrum of modes, some of which can involve highly excited states. We quantify the performance of our system by the entanglement rate, which is exact beyond the weak excitation regime and upper-bounds the performance of any practical entanglement distribution protocol. Our simulation demonstrates robust and efficient entanglement creation without requiring cavity impedance matching, parameter fine tuning or strong coupling. Even with an imperfect intra-cavity photon-memory transfer and discarding the signal photons, we see no significant degradation of bipartite entanglement between the memory and the idler photons.

We further describe experimental realizations using existing technologies based on photonic microcavities coupled to ensembles of rare-earth ions doped in a crystalline substrate. The proposed system is capable of generating up to 50 MHz Ebits over a range of accessible experimental parameters. The high Ebit generation rate is result of a large number of frequency modes within the inhomogeneous linewidth of the memory, and the accurate accounting of entanglement in the strongly driven regime. Our proposal is distinct from the DLCZ protocol with its quasi-CW, multimode operation, while it eliminates the loss and mismatch challenges in pair-source based repeater protocols [11]. Furthermore, the intrinsic tri-partite nature of the entanglement - between two photonic and one memory degrees of freedom - opens future opportunities of generating and distributing multi-partite entanglement over a network for quantum secret sharing [16, 17], multi-partite teleportation [18], and distributed sensing [19].

*Entanglement generation.*- Our entanglement generation process can be modelled as two cavity modes, signal ( $\hat{B}_S$ ) and idler ( $\hat{B}_I$ ), which are spectrally distinct, and which couple independently to a common waveguide with

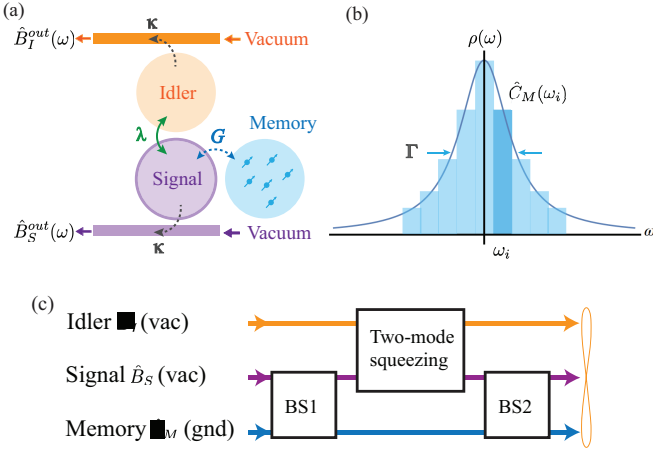


FIG. 1. (a) Generalized model of three-mode system: Entangled signal ( $\hat{B}_S$ ) and idler ( $\hat{B}_I$ ) are generated by parametric driving and signal is coupled to spin memory ( $\hat{C}_M$ ) (b) Spectral slicing of inhomogeneously broadened atomic ensemble memory. (c) Equivalent circuit consists of one two-mode-squeezing gate sandwiched by two beam-splitters. The amount of output excitation is characterized by the TMS strength  $\cosh^2 r$ . The second beam-splitter (BS2), which determines the amount of entanglement or photon going into memory, has a beam-splitting angle  $\theta_2$ . The first beam splitter (BS1), which has a beam-splitting angle  $\theta_1$ , is irrelevant for our situation of vacuum/ground state input.

a coupling rate  $\kappa$ . The waveguide frequency mode, that is detuned by  $\omega$  from the signal (idler) mode frequency, is represented by  $\hat{b}_{S\omega}$  ( $\hat{b}_{I\omega}$ ). The signal mode also couples to an atomic ensemble memory with a spectral distribution  $\rho(\omega)$ . In the rotating frame of the cavity modes the Hamiltonian of the system is

$$\hat{H} = \lambda(\hat{B}_S^\dagger \hat{B}_I^\dagger + \hat{B}_S \hat{B}_I) + \int \omega \hat{c}_{M\omega}^\dagger \hat{c}_{M\omega} d\omega + G \int \sqrt{\rho(\omega)} (\hat{B}_S^\dagger \hat{c}_{M\omega} + \hat{c}_{M\omega}^\dagger \hat{B}_S) d\omega, \quad (1)$$

where  $G$  is the collective atom-photon coupling. In our protocol the device is driven by a constant intensity pump at the frequency  $\omega_p = (\omega_S + \omega_I)/2$  from  $t = t_o$  to  $t = t_f$ , this will induce a parametric drive with strength  $\lambda$  in the cavities. Generally, atoms with the frequencies within the ‘strip’  $\omega$  to  $\omega + d\omega$  are not resolvable if  $d\omega$  is much smaller than the resolvable bandwidth  $\delta_r \equiv 1/(t_f - t_o)$ . We consider the ensemble has a wide inhomogeneous broadening  $\Gamma \gg \delta_r$ , so the atomic excitation within each strip can be represented by the collective bosonic operator  $\hat{c}_{M\omega}^\dagger$ , and the collective spin-photon coupling of each strip is scaled by  $\sqrt{\rho(\omega)}$  [20]. We note that this representation is compatible with holeburning memory protocols such as atomic frequency combs [21], in which the comb spacing  $\Delta$  cannot be resolved during the pump time, i.e.  $\delta_r \gg \Delta$ , and the ensemble can be effectively modelled with a modified atomic density.

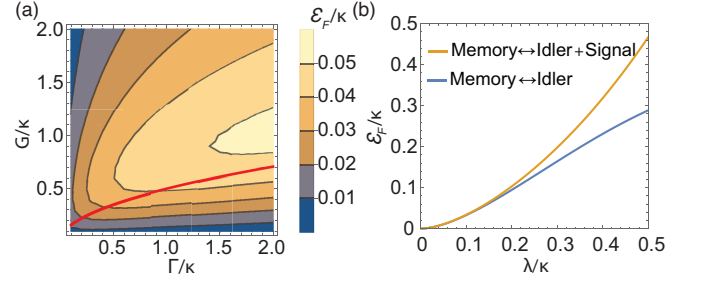


FIG. 2. (a) Normalized entanglement rate  $\mathcal{E}_F/\kappa$  as a function of the coupling  $G$  and the atomic ensemble linewidth  $\Gamma$  while keeping a weak parametric drive at  $\lambda = 0.1\kappa$ . The cavity impedance matching condition is also plotted as in red curve. (b) Normalized entanglement rate  $\mathcal{E}_F/\kappa$  as a function of parametric drive  $\lambda/\kappa$ . Here we assumed  $2G = \Gamma = \kappa$ , so  $\mathcal{C} = 1$ . Orange (Blue) curve represents the entanglement between memory and idler output only (both signal and idler output).

For sufficiently long drive, i.e.  $t_f - t_o \gg 1/\kappa$ , the output photonic modes and atoms can be characterized by the steady-state scattering relation

$$\begin{aligned} \hat{B}_I^{\text{out}\dagger}[\omega] &= T_{II} \hat{B}_I^{\text{in}\dagger}[\omega] + T_{IS} \hat{B}_S^{\text{in}}[\omega] + T_{IM} \hat{C}_M^{\text{in}}[\omega] \\ \hat{B}_S^{\text{out}}[\omega] &= T_{SI} \hat{B}_I^{\text{in}\dagger}[\omega] + T_{SS} \hat{B}_S^{\text{in}}[\omega] + T_{SM} \hat{C}_M^{\text{in}}[\omega] \\ \hat{C}_M^{\text{out}}[\omega] &= T_{MI} \hat{B}_I^{\text{in}\dagger}[\omega] + T_{MS} \hat{B}_S^{\text{in}}[\omega] + T_{MM} \hat{C}_M^{\text{in}}[\omega]. \end{aligned} \quad (2)$$

We note that the scattering amplitudes  $T$  depend on detuning  $\omega$ , which is omitted in the above equations only for brevity. The input/output operators of the photonic waveguide follow the standard definitions,  $\hat{B}_u^{\text{in}/\text{out}}(t) \equiv \frac{1}{\sqrt{2\pi}} \int \hat{b}_{u\omega}(t_o/t_f) e^{-i\omega(t-t_o/t_f)} d\omega$ , for  $u = S, I$ . Analogously, we can define the effective input and output operators of atoms as  $\hat{C}_M^{\text{in}/\text{out}}(t) \equiv \frac{1}{\sqrt{2\pi}} \int \hat{c}_{M\omega}(t_o/t_f) e^{-i\omega(t-t_o/t_f)} d\omega$ , which characterizes the transformation of the atomic state before and after interacting with the cavity.

This scattering relation shows that our system intrinsically generates tri-partite entanglement between each frequency mode of idler, signal, and memory. The equivalent circuit is depicted in Fig. 1(c), which involves two beam splitters (BS) with the same angle  $\tan \theta_1 = \left| \frac{T_{IM}(\omega)}{T_{IS}(\omega)} \right| = \tan \theta_2 = \left| \frac{T_{MI}(\omega)}{T_{SI}(\omega)} \right|$ , and a two-mode-squeezing (TMS) interaction with strength  $\cosh^2 r = |T_{II}(\omega)|^2$ . We note that the mode transformation denoted by Eq. (2) applies to any input state, so our setup can also be applied to engineering logic gates between itinerant photons and quantum states stored in the memory [22]. For our current goal of in-situ generation of photon-memory entanglement, we assume both signal and idler inputs are vacuum and the memory is initialized in the ground state.

To quantify the amount of entanglement, we consider a Lorentzian spectrum,  $\rho(\omega) = \frac{\Gamma}{2\pi \omega^2 + (\Gamma/2)^2}$ , with  $\omega$  defined as the detuning from atomic ensemble fre-

quency with an inhomogeneous broadening  $\Gamma$ . Based on the equivalent circuit in Fig. 1(c), one might guess that a complete transfer of the entangled signal photon to the memory necessarily requires a large effective beam splitting angle

$$\tan^2 \theta_2 = \left| \frac{T_{MI}(\omega)}{T_{SI}(\omega)} \right|^2 = \frac{\mathcal{C}}{1 + 4\omega^2/\Gamma^2}. \quad (3)$$

This would require in turn a large collective atomic ensemble-cavity cooperativity  $\mathcal{C} \equiv 4G^2/\kappa\Gamma \gg 1$ . We find however that this condition is neither necessary nor optimal for our memory. Heuristically, increasing  $\mathcal{C}$  enhances the effective damping of the cavity, which is harmful as it suppresses photon generation due to the parametric drive.

Further, our analysis indicates that there is no special utility in achieving impedance matching (i.e.  $\mathcal{C} = 1$ ): we thus conclude that fine tuning to reach this matching is not required. To be more specific, we quantify the performance of our protocol by the entanglement rate  $\mathcal{E}_R$ , which is the total amount of photon-memory entanglement generated in all frequency modes per unit time [23, 24]:

$$\mathcal{E}_R \equiv \frac{\sum_{\omega} \mathcal{E}_F(\omega)}{\tau_{\text{pump}}} \approx \frac{1}{2\pi} \int \mathcal{E}_F(\omega) d\omega. \quad (4)$$

Here  $\tau_{\text{pump}}$  is the pump time, and  $\mathcal{E}_F(\omega)$  is the entanglement of formation of the frequency mode at  $\omega$ , which can be computed exactly as the output state is Gaussian and balanced [25]. We note that the entanglement of each mode can be directly summed because the total system output state is a tensor product of each frequency mode state. Our choice of  $\mathcal{E}_R$  as entanglement quantifier is advantageous as it does more than account for the entanglement associated with single excitations: contributions from vacuum and highly excited states are also fully included. Furthermore, it represents the device's maximum performance in entanglement generation for a fixed choice of system parameters, i.e. any post-selection or non-Gaussian process cannot improve the rate of entanglement generation.

Fig. 2(a) plots the memory-idler entanglement rate  $\mathcal{E}_R$  as a function of both the atomic ensemble linewidth and the ensemble-cavity coupling. For maximizing  $\mathcal{E}_R$ , it is clear that impedance matching is neither necessary nor universally optimal. We also observe that around the regime of maximum performance, the value of  $\mathcal{E}_R$  is robust against order-unity changes in system parameters. This is ultimately because the memory captures the entangled photon directly from the signal cavity, a process that can occur efficiently without the fine tuning that would be required if instead photons had to be captured from a waveguide.

The above analysis considered memory-idler photon entanglement assuming that outgoing signal photons are

discarded. One might worry that this discarding results in a significant loss of entanglement, especially since the effective beam splitting angle in Eq. (3) is not overwhelmingly large at the parameters of maximum performance in Fig. 2(a) (i.e.  $\mathcal{C}$  is of order unity). To investigate this concern, we compare in Fig. 2(b) the entanglement rate for two cases: (i) between memory and both photonic (signal and idler) outputs (computed using the entropy of the final memory state); (ii) between memory and idler output only, with the signal output discarded. Interestingly, the photon-memory entanglement rate is barely degraded when the drive is weak (i.e.  $\lambda \ll \kappa$ ), and shows only about a factor of two reduction when  $\lambda$  is comparable to  $\kappa$  (instability occurs when  $\lambda \rightarrow \kappa/\sqrt{2}$  in our choice of parameters [20]). The intuition behind this effect is that the entanglement rate has significant contributions from off-resonant modes (i.e.  $\omega \neq 0$ ). These modes are only weakly excited even when the resonant mode is driven close to instability. On the other hand, idler-memory entanglement would only be destroyed when a photon is detected in signal output. Since the signal output of off-resonant modes contain mainly vacuum, there is a high probability that the idler-memory entanglement is retained even if signal is monitored or discarded. Nevertheless, despite the weak excitation, the tri-partite entanglement between idler, signal and memory is genuine and can be harnessed as a resource for quantum information applications [16–19].

*Experimental scheme.*— The proposed in-situ entanglement generation can be realized experimentally with existing technologies. We design an integrated device that consists of a silicon micro-ring resonator on top of a  $^{167}\text{Er}^{3+}:\text{Y}_2\text{SiO}_5$  crystalline substrate, as shown in Fig. 3. Entangled signal and idler photon pairs are generated by spontaneous four-wave-mixing (sFWM) in the silicon micro-ring resonator with an estimated MHz generation rate at  $\mu\text{W}$  pump power [26, 27] [20]. The on-chip resonator implementation with micron-scale ring diameter is necessary as it provides sufficiently large (e.g.  $\approx 5$  nm) free spectral range so that the signal, idler and pump photons are well separated over 3 resonance modes [20]. The signal cavity mode is resonant with the  $^{167}\text{Er}^{3+} : \text{YSO}$  optical transition at 1538 nm, between the ground and excited-state  $|7/2\rangle_{e-g}$  hyperfine levels [28]. Assuming a doping concentration of 50 parts per million (ppm), the evanescent coupling between the transverse magnetic (TM) mode of the resonator and the Er ensembles leads to a collective coupling strength of  $G = 0.3$  GHz [20].

The quantum memory protocol we propose is based on optical atomic frequency combs (AFC), which have built-in multimode capability [21]. A long-lived AFC is first prepared by initializing and holeburning on the  $^{167}\text{Er}^{3+}$  ensemble prior to entanglement generation. Then a quasi-CW pump laser is turned on with a time duration  $\tau_{\text{pump}} \gg 1/\kappa$  to continuously generate entangled photons in idler and signal cavities. If there is no memory,

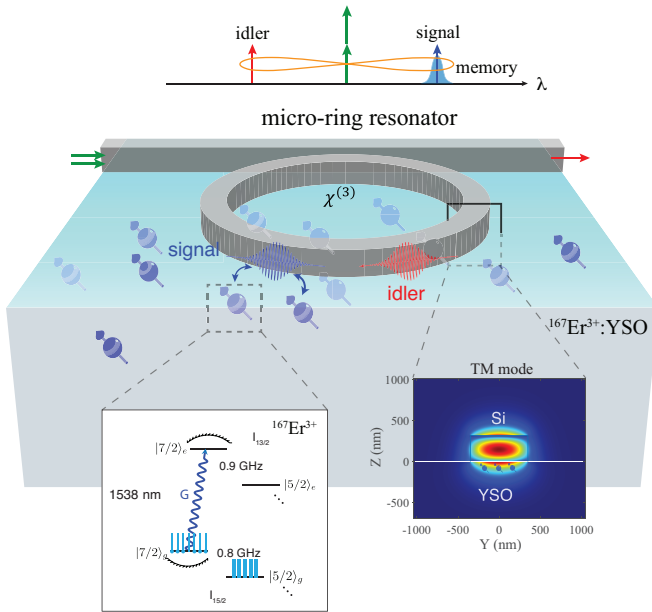


FIG. 3. Experimental realization of in-situ entanglement generation based on a microring resonator on Er:YSO crystal. The  $^{167}\text{Er}^{3+}$  ions are evanescently coupled to optical field confined in a Si waveguide. A pump field (green) generates entangled signal (blue) and idler (red) photons pairs via sFWM process while signal photons are coupled with Er optical transitions and the idler photons are coupled out of the cavity to the waveguide. Left inset shows the quantum memory scheme based on AFC and the relevant  $^{167}\text{Er}^{3+}$  energy levels. Right inset shows the simulation of transverse magnetic mode profile of Si waveguide on a  $^{167}\text{Er}^{3+}$ : YSO substrate.

the output is a continuum of entangled photon with frequency centered at  $\omega_I$  and  $\omega_S$  respectively, which can also be viewed as a continuous stream of temporally (or time-energy) entangled photons with the duration of each defined by the cavity lifetime  $1/\kappa$ . In our scheme that involves additionally the memory, photons in the signal cavity mode are stored into the AFC with a storage time  $T_M = 1/\Delta$  where  $\Delta$  is the AFC comb spacing. We further require that the pump duration is shorter than the storage time, so that our ensemble description of the memory remains valid.

AFC memory storage efficiency in our scheme is determined by Eq. (3), in which the effective cooperativity should take into account the finesse of the AFC:  $F_{\text{AFC}} = \Delta/\gamma$ , where  $\gamma$  is the spectral width of the comb tooth. For  $^{167}\text{Er}$ :YSO, a storage time of  $1\mu\text{s}$  is achievable, with a AFC finesse  $F_{\text{AFC}}=3$ ,  $\Delta=1$  MHz, and  $\gamma \approx 0.3$  MHz [29, 30]. Long-term storage is feasible with spin-wave memory using an additional hyperfine level [28]. While the signal photons are stored, the idler photons are propagating out of the cavity. The average idler photon number in each temporal mode is controlled by adjusting the pump strength  $\lambda$ . We stress that the entanglement generated in our scheme can be accounted for even when

TABLE I. Example experimental parameters

$\Gamma$ (MHz)	$G$ (GHz)	$\kappa$ (MHz)	$\lambda$ (MHz)	$F_{\text{AFC}}$	$T_M$ ( $\mu\text{s}$ )
150	0.3	150	40	3	1

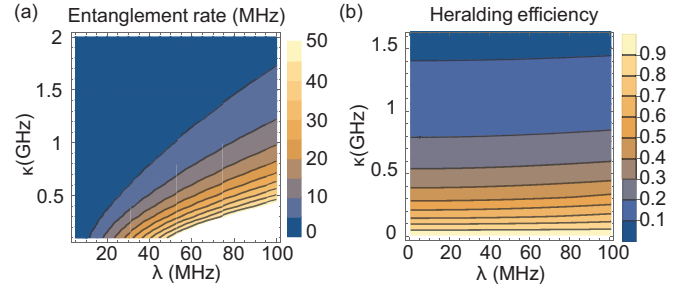


FIG. 4. (a) Entanglement rate  $\mathcal{E}_R$  of generated photon-memory pair and (b) Heralding efficiency  $\eta$ . System parameters are given in Table I.

$\lambda$  is large.

*Entanglement rate.* - We first analyze the entanglement rate of our experimental setup. Remote entanglement generation with separate photon pair source and quantum memory has demonstrated heralded entanglement rate up to 15.6 kHz [12], which is mainly limited by a low photon pair generation rate, high loss and signal photon storage inefficiency. Our in-situ scheme can circumvent the limitations of interface loss and storage inefficiency through directly coupling to memory. Furthermore, the entanglement rate  $\mathcal{E}_R$  takes into account the entanglement of higher excited states, so the performance of our setup can be faithfully quantified even the cavity is strongly driven.

In Fig. 4(b) with a fixed coupling  $G = 0.3$  GHz, we show the entanglement rate at varying parametric drive  $\lambda$  and cavity decay rate  $\kappa$ . The peak entanglement rate can reach as much as 50 MHz Ebits. For the example experimental parameters in Table I, the entanglement rate with a  $\lambda=40$  MHz is 30.3 MHz. This high Ebit rate is achieved when the cavity is driven just below the instability threshold, i.e. the white region in Fig. 4(b). We note that although the resonant frequency mode will be highly excited near the threshold, the time-bin mode that is addressed by usual time-resolved detectors contains much less than one photon on average, due to the contribution of the off-resonant frequency modes which are weakly excited. This combination of in-situ generation and accounting the full structure of entanglement shows that our setup has the potential to achieve orders of magnitude higher rates than that of latest experiments in [12, 13].

*Heralding efficiency.*- The inherently continuous-variable entanglement in our scheme can also be a useful resource for applications based on discrete-variable encoding. One use case is heralded entanglement gen-

eration in a quantum repeater network, in which detection of a single itinerant photon heralds the storage of a qubit in the memory. We next analyze the heralding efficiency as an important figure of merit in such context. Previously, Ref. [31] demonstrated heralded single-photon source with 83% heralding efficiency. However, this efficiency would be much lower if one needs to store the photon into separate quantum memory (19% demonstrated in [12] and 14.3% AFC efficiency in a two-photon-detection heralded entanglement distribution experiment [13]). We thus define the heralding efficiency as rate of non-zero memory excitation to the output rate of non-zero idler photon,

$$\eta \equiv \frac{\int \left(1 - \frac{1}{1+|T_{MI}(\omega)|^2}\right) d\omega}{\int \left(1 - \frac{1}{1+|T_{IS}(\omega)|^2+|T_{IM}(\omega)|^2}\right) d\omega}. \quad (5)$$

It indicates the efficiency that signal photon has been stored in the memory given the detection of idler photon coming out of the cavity.

We plot the heralding efficiency as a function of  $\kappa$  and  $\lambda$  in Fig. 4(a). With a fixed  $G = 0.3$  GHz, heralding efficiency up to 90% can be achieved with a  $\kappa < 50$  MHz or a cavity quality factor  $Q > 4 \times 10^6$ , which has been demonstrated with silicon microring resonators [32]. With more practical parameters in Table I, we still obtain a high heralding efficiency of 70%.

*Summary.*- We have presented a scheme for in-situ generation of entanglement between itinerant optical photons and quantum memories and describe an experimental realization based on existing technologies. By eliminating loss associated with the photon-memory interfaces while retaining the multimode feature of the ensemble-based memories, we demonstrate a system capable of generating robust, 10s MHz-rate, bi-party entanglement between optical photons and atomic memories without stringent impedance matching or fine parameter tuning.

Future work will consider remote entanglement of two such systems via entanglement swap of both idler photons from adjacent memory nodes in a network, and the impact of channel loss on the entanglement rate. Photon retrieval from the memories will also need to be optimized, for instance by actively tuning the cavity Q or resonance frequency via carrier injection into a Si waveguide [33] for a high retrieval efficiency. The general framework of our proposal can be extended to a variety of hybrid quantum systems. With ensembles of spins in solids, coupling to superconducting resonators with a modest non-linearity would enable high-rate microwave-memory entanglement. Similar idea is applicable to optomechanics to generate photon-phonon entanglement [34–36], and to magneto-optical systems for photon-magnon entanglement [37–39]. Finally, the intrinsic three-mode entangling operation in our scheme also opens a future avenue to engineer multi-mode logic gates, as well as create and

distribute hybrid multi-party entanglement across a network for advanced quantum communication and sensing protocols.

We acknowledge useful discussions with Kurt Jacob. This work was funded by a National Science Foundation (NSF) Faculty Early Career Development Program (CAREER) Grant (No. 1944715), partially supported by the University of Chicago Materials Research Science and Engineering Center, which is funded by the National Science Foundation under award number DMR-2011854, and the NSF QLCI for Hybrid Quantum Architectures and Networks (NSF Grant No. 2016136). H.-K.L. acknowledges partial support from Canada Research Chairs.

- 
- [1] H. J. Kimble, *Nature* **453**, 1023 (2008).
  - [2] S. Wehner, D. Elkouss, and R. Hanson, *Science* **362**, eaam9288 (2018).
  - [3] J. I. Cirac, P. Zoller, H. J. Kimble, and H. Mabuchi, *Phys. Rev. Lett.* **78**, 3221 (1997).
  - [4] N. J. Lambert, A. Rueda, F. Sedlmeir, and H. G. L. Schwefel, *Advanced Quantum Technologies* **3**, 31900077 (2019).
  - [5] M. Mirhosseini, A. Sipahigil, M. Kalaei, and O. Painter, *Nature* **588**, 599 (2020).
  - [6] D. Gottesman, T. Jennewein, and S. Croke, *Physical review letters* **109**, 070503 (2012).
  - [7] L. K. Grover, arXiv preprint quant-ph/9704012 (1997).
  - [8] L. Jiang, J. M. Taylor, A. S. Sørensen, and M. D. Lukin, *Phys. Rev. A* **76**, 062323 (2007).
  - [9] C. Monroe, R. Raussendorf, A. Ruthven, K. R. Brown, P. Maunz, L.-M. Duan, and J. Kim, *Phys. Rev. A* **89**, 022317 (2014).
  - [10] L.-M. Duan, M. D. Lukin, J. I. Cirac, and P. Zoller, *Nature* **414**, 413 (2001).
  - [11] C. Simon, H. de Riedmatten, M. Afzelius, N. Sangouard, H. Zbinden, and N. Gisin, *Physical Review Letters* **98**, 190503 (2007).
  - [12] D. Lago-Rivera, S. Grandi, J. V. Rakonjac, A. Seri, and H. de Riedmatten, *Nature* **594**, 37 (2021).
  - [13] X. Liu, J. Hu, Z.-F. Li, X. Li, P.-Y. Li, P.-J. Liang, Z.-Q. Zhou, C.-F. Li, and G.-C. Guo, *Nature* **594**, 41 (2021).
  - [14] M. Afzelius and C. Simon, *Physical Review A* **82**, 022310 (2010).
  - [15] S. A. Moiseev, S. N. Andrianov, and F. F. Gubaidullin, *Physical Review A* **82**, 022311 (2010).
  - [16] T. Tyc and B. C. Sanders, *Physical Review A* **65**, 042310 (2002).
  - [17] H. K. Lau and C. Weedbrook, *Physical Review A* **88**, 042313 (2013).
  - [18] Y. Lian, C. Xie, and K. Peng, *New Journal of Physics* **9**, 314 (2007).
  - [19] Q. Zhuang, Z. Zhang, and J. H. Shapiro, *Physical Review A* **97**, 032329 (2018).
  - [20] See the Supplemental Material for more details.
  - [21] M. Afzelius, C. Simon, H. De Riedmatten, and N. Gisin, *Physical Review A* **79**, 052329 (2009).
  - [22] H.-K. Lau and A. A. Clerk, *npj Quantum Information* **5**,

- 31 (2019).
- [23] Z. Jiao Deng, S. J. M. Habraken, and F. Marquardt, *New Journal of Physics* **18**, 063022 (2016).
- [24] C. Zhong, X. Han, H. X. Tang, and L. Jiang, *Physical Review A* **101**, 032345 (2020).
- [25] S. Tserkis and T. C. Ralph, *Physical Review A* **96**, 062338 (2017).
- [26] S. Azzini, D. Grassani, M. J. Strain, M. Sorel, L. G. Helt, J. E. Sipe, M. Liscidini, M. Galli, and D. Bajoni, *Optics Express* **20**, 23100 (2012).
- [27] W. C. Jiang, X. Lu, J. Zhang, O. Painter, and Q. Lin, *Optics Express* **23**, 20884 (2015).
- [28] M. Rančić, M. P. Hedges, R. L. Ahlefeldt, and M. J. Sellars, *Nature Physics* **14**, 50 (2018).
- [29] S. Yasui, M. Hiraishi, A. Ishizawa, H. Omi, R. Kaji, S. Adachi, and T. Tawara, *Opt. Express* **29**, 27137 (2021).
- [30] I. Craiciu, M. Lei, J. Rochman, J. M. Kindem, J. G. Bartholomew, E. Miyazono, T. Zhong, N. Sinclair, and A. Faraon, *Phys. Rev. Applied* **12**, 024062 (2019).
- [31] S. Ramelow, A. Mech, M. Giustina, S. Gröblacher, W. Wieczorek, J. Beyer, A. Lita, B. Calkins, T. Ger-  
rits, S. W. Nam, A. Zeilinger, and R. Ursin, *Optics Express* **21**, 6707 (2013).
- [32] B. Zhang, K. A. Qubaisi, M. Cherchi, M. Harjanne, Y. Ehrlichman, A. N. Khilo, and M. A. Popović, *Opt. Lett.* **45**, 3005 (2020).
- [33] Q. Xu, B. Schmidt, S. Pradhan, and M. Lipson, *Nature* **435**, 325 (2005).
- [34] Y.-D. Wang, S. Chesi, and A. A. Clerk, *Physical Review A* **91**, 013807 (2015).
- [35] A. Wallucks, I. Marinković, B. Hensen, R. Stockill, and S. Gröblacher, *Nature Physics* **16**, 772 (2020).
- [36] C. Zhong, Z. Wang, C. Zou, M. Zhang, X. Han, W. Fu, M. Xu, S. Shankar, M. H. Devoret, H. X. Tang, and L. Jiang, *Physical Review Letters* **124**, 010511 (2020).
- [37] H. Tanji, S. Ghosh, J. Simon, B. Bloom, and V. Vuletić, *Physical Review Letters* **103**, 043601 (2009).
- [38] J. Simon, H. Tanji, S. Ghosh, and V. Vuletić, *Nature Physics* **3**, 765 (2007).
- [39] L. A. Williamson, Y.-H. Chen, and J. J. Longdell, *Physical Review Letters* **113**, 203601 (2014).